Optical characteristics of the EUV spectrometer (EUS) for SOLO

L. Poletto, G. Tondello
INFM - Istituto Nazionale per la Fisica della Materia
Department of Electronics and Informatics, University of Padova
via Gradenigo 6/A - 35131 Padova (Italy)

November, 2001

1. Introduction

The optical design and performance of a stigmatic telescope-spectrometer for high-resolution solar imaging spectroscopy in the spectral region 1160-1260 Å (580-630 Å) is presented. The aim of this work is to give a preliminary estimation of the performance of an instrument to be accommodated on SOLO.
At Tenerife, it has been discussed the possibility of having a spectrometer with diagnostic capabilities both on the chromosphere (with lines longward of the H edge at 912 Å) and on the transition region (with lines around 600 Å). One option is to set up a design which uses the first order 1160-1260 Å band with 580-630 Å in the second order.
At the present, the EUV spectroscopic instrumentation proposed for SOLO consists of a normal-incidence high-resolution spectrometer (EUS-EUV Spectrometer). The basic optical layout is a Ritchey-Chretien telescope that feeds a toroidal-grating spectrometer optimized for the 58-62 nm range in the first diffracted order. The grating is expected to give spectral images also in the second diffracted order around 30 nm. Since the reflectivity of conventional coatings at normal incidence is few % at 30 nm, the detection of the second diffracted order requires multilayer coatings. Unfortunately, the severe thermal environment of the mission makes it very difficult to use multilayer coatings on optics looking directly at the solar disk (the average solar intensity at 0.2 AU is ≈34 kW/m^2). The EUS without multilayer optics is then limited only to the normal-incidence region (i.e. for wavelengths longer than ≈350 Å).
This optical design can be modified in order to match the requirements of an extended band of operation, at 1200 Å in the first order and 600 Å in the second order. Conventional metallic coatings have rather high reflectivity even at normal incidence in such a wide spectral region.
Here, three different configurations will be analyzed and compared:

Configuration A. A normal-incidence telescope feeding a normal-incidence toroidal-grating spectrometer;
Configuration B. A normal-incidence telescope feeding a normal-incidence variable-line-spaced-grating (VLS) spectrometer;
Configuration C. A grazing-incidence telescope feeding a normal-incidence VLS-grating spectrometer.

Although each configuration is formed by two sections (the telescope and the spectrometer), the optical performance have to be evaluated by taking into account the whole of the two parts. For example, the very high spatial resolution given by a two-element telescope in a wide field-of-view can be unacceptably degraded by the following single-element spectrometer.
Three essential optical parameters have to be calculated in the evaluation of the optical performance of a telescope-spectrometer: 1) the spatial resolution in the direction perpendicular to the entrance slit, which depends only on the optical properties of the telescope; 2) the spectral resolution and 3) the spatial resolution in the direction parallel to the slit, which on the contrary depend on the performance of the whole instrument (telescope + spectrometer).
Note that a single-element optic, although at normal incidence, has off-axis aberrations that can not be eliminated, but only reduced by minimizing the subtended angle. Then, the grating spectrometer introduces additional aberrations that have to be carefully analyzed.

2. Configuration A: normal-incidence telescope and normal-incidence toroidal-grating spectrometer

The configuration A is essentially the strawman configuration. It consists of a Ritchey-Chretien telescope with 34 arcmin field-of-view that feeds a toroidal-grating spectrometer optimized for the 1160-1260 Å (580-630 Å) range in the first (second) diffracted order. In the current design, the primary and secondary mirrors are separated by 900 mm, with the focal plane 200 mm beyond the primary. The effective focal length is about 3.7 m. The intrinsic resolution of the telescope is very good: it has been verified that the spot size on the slit plane is lower than 10 μm within the whole field-of-view. Giving a slit width of 9 μm, the region of the Sun imaged on the detector is a rectangular portion with angular size 0.5 arcsec (perpendicular to the slit) × 34 arcmin (parallel to the slit). The spatial resolution in the direction perpendicular to the slit is then 0.5 arcsec in the whole field-of-view. Furthermore, it has been verified that the

secondary mirror can be rotated to allow rastered images, i.e. successive acquisitions to build monochromatic two-dimensional images. This has the advantage of requiring no additional mirror for the rastering.
Instead, the spectral resolution and the spatial resolutions in the direction parallel to the slit are limited by the grating performance. The toroidal grating has a groove density of 2400 lines/mm and is optimized in the region 1160-1260 Å (580-630 Å) in the first (second) order. The spectrometer works with a magnification of 1.5 (off-Rowland configuration), with entrance arm of 1200 mm and exit arm of 1760 mm, corresponding to a spectral dispersion of 2.37 (1.18) Å/mm in the first (second) order. The extension of the spectrum is 42 mm (in the direction of spectral dispersion) × 54 mm (in the direction parallel to the slit). This requires a detector array of 2800 × 3600 15 μm pixel. The spectral resolving element is 35.5 (17.8) mÅ in the first (second) order, which corresponds to a velocity resolution of about 8.8 km/s. The spatial resolving element is 0.55 arcsec. Note that the velocity resolution can be increased by the centroiding.
A schematic layout of the optical configuration is shown in Fig. 1. The parameters of the telescope-spectrometer are summarized in Tab. 1.
The resolution perpendicular to the slit within the field-of-view is shown in Fig. 2. It is almost constant to 0.5 arcsec (75 km on the Sun at 0.2 AU) with a 9 μm slit. Note that the resolution depends only on the double-element telescope and is not degraded by the presence of an additional optical element.
The spectral and spatial aberrations (calculated with the criterion of the 80% of the encircled energy) on the focal plane of the spectrometer are shown in Fig. 3. They have been calculated by simulating the whole optical system (telescope + spectrometer).

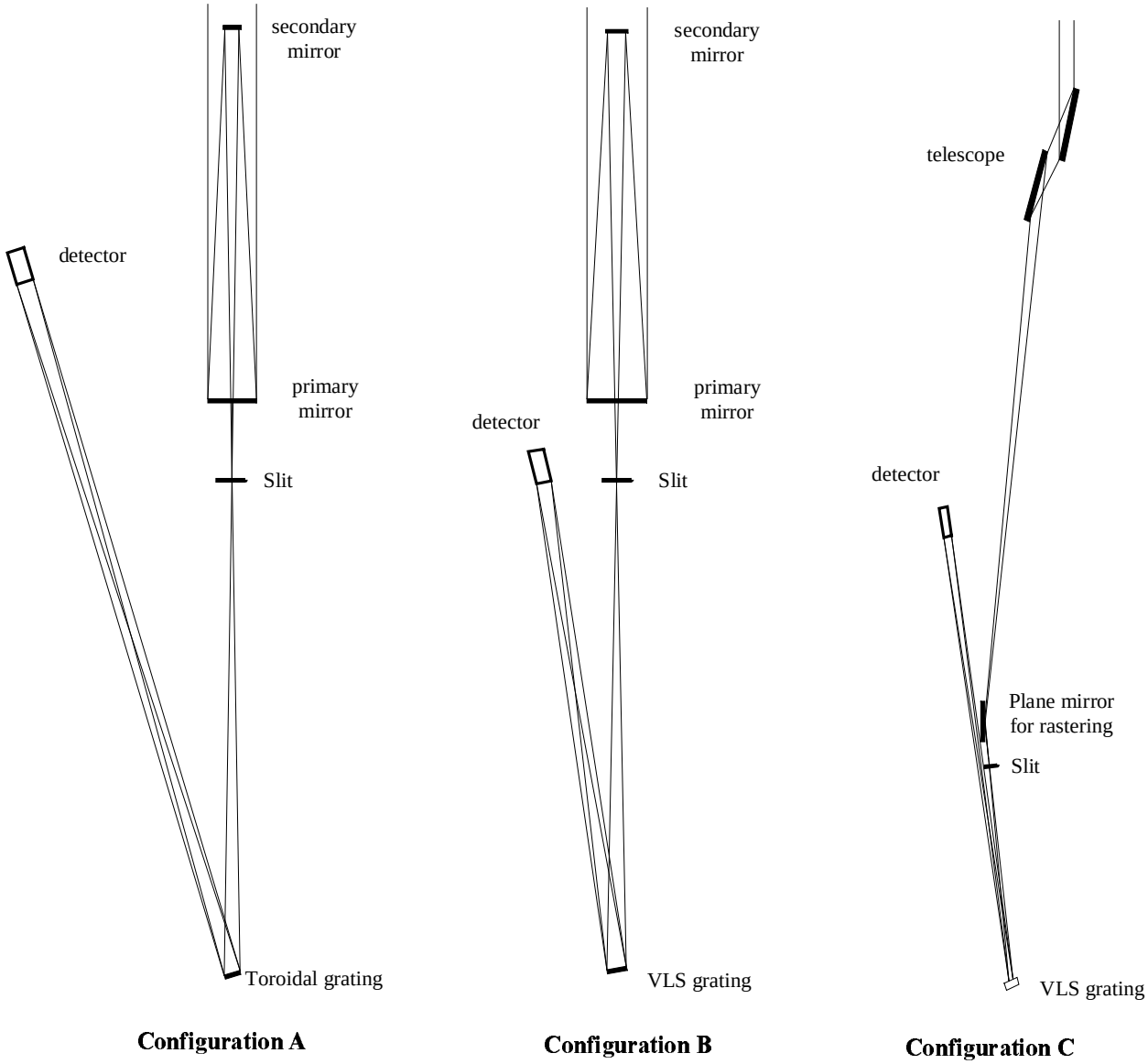

Fig.1. Optical layout of the configurations A, B (normal-incidence) and C (grazing-incidence).

Telescope	Ritchey-Chretien
Field of view	34 arcmin (parallel to the slit, simultaneous) × 34 arcmin (⊥ to the slit, to be acquired by rastering)
Telescope tube	
Diameter	130 mm
Length	1000 mm
Primary mirror	
Diameter	120 mm
Secondary mirror	
Distance from the primary	900 mm
Extraction length	200 mm
Diameter	45 mm
Focal length	3700 mm
Slit	
Size	9 μm × 36 mm
Spatial resolution ⊥ to the slit	0.5 arcsec
Grating	Toroidal
Groove density	2400 lines/mm
Wavelength of operation	1160-1260 Å (first order) 580-630 Å (second order)
Entrance arm	1200 mm
Exit arm	1760 mm
Incidence angle	16.88°
Tangential radius	1470 mm
Sagittal radius	1397 mm
Size	40 mm (⊥ to the grooves) × 105 mm
Coating	SiC
Detector	
Pixel size	15 μm
Format	2800 pixel × 3600 pixel
Area	42 mm (⊥ to the slit) × 54 mm
Spectral resolving element	36 mÅ (I order)
Spatial resolving element	0.55 arcsec

Tab. 1. Characteristics of the telescope-spectrometer in configuration A

The spectral aberrations are constant within the spectral region to be acquired. The on-axis aberrations with a 9 μm slit are about 15 μm, because of the combined effects of the grating magnification and the residual aberrations due to the off-Rowland configuration. Unfortunately, both spectral and spatial aberrations are considerably degraded for off-axis points. Despite the high performance of the Ritchey-Chretien telescope on the slit plane, the actual spectral and spatial resolutions are limited by the grating aberrations, because a single-element spectrometer has large off-axis aberrations that can not be corrected. In particular, the spectral and spatial resolutions are respectively degraded to 550 mÅ and 9 arcsec at ±17 arcmin. Then, the resolution is not preserved within the field-of-view, with a degradation up to a factor 15-20 with respect to the nominal performance.

The large off-axis aberrations are essentially due to the large subtended angle on the grating. The incidence angle, in case of using a toroidal grating, has been chosen in order to have a central diffraction angle equal to zero (i.e. $\beta = 0$ for $\lambda = 1210$ Å); this implies minimal spectral aberrations within the range to be acquired. Lower off-axis aberrations can be obtained by using a lower incidence angle, but without constant spectral resolution within the whole spectral region to be acquired.

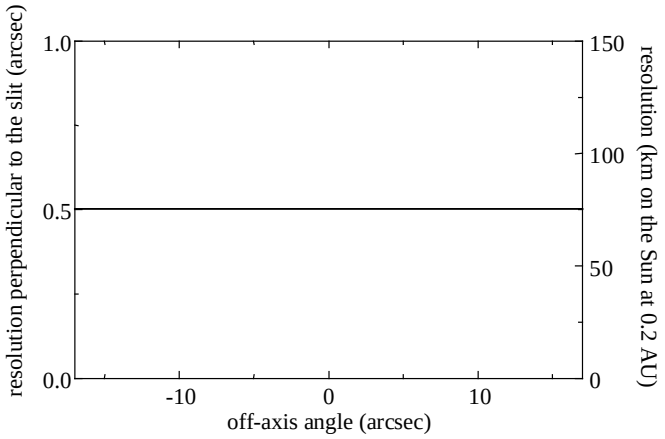

Fig. 2. Configuration A: spatial resolution perpendicular to the slit (9 μm wide). The resolution is almost constant with the rastering. The aberrations in the direction perpendicular to the slit depend only on the telescope.

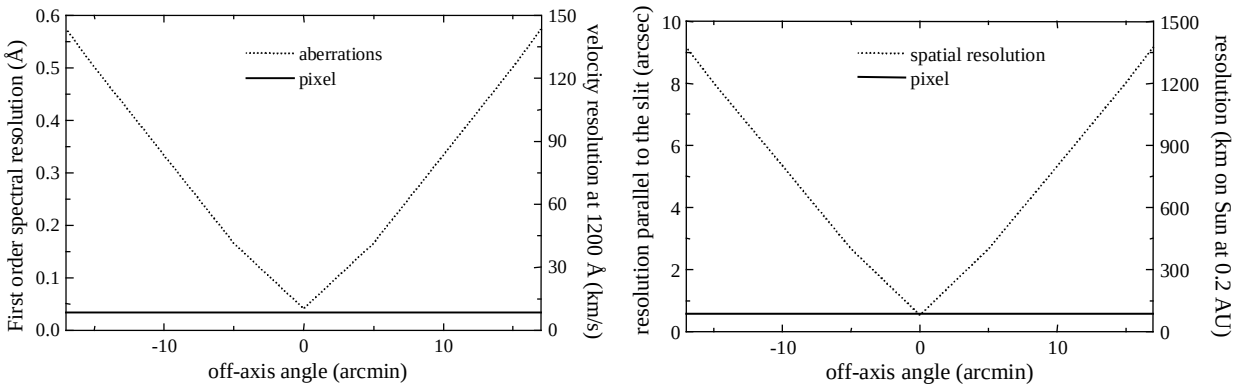

Fig. 3. Configuration A: spectral resolution and spatial resolution parallel to the slit. The pixel size is 15 μm. The resolutions have been obtained by a simulation of the whole instrument.

3. Configuration B: normal-incidence telescope and normal-incidence VLS-grating spectrometer

An alternative configuration to the Rowland design with toroidal gratings is that using spherical VLS gratings. By using a proper distribution of the line spacing the spectral curve can be brought to intersect the straight line in one or two points, obtaining so an extended stigmatic spectral region. The stigmatic incidence angle in case of using a VLS grating is lower than the conventional Rowland mounting, so also lower off-axis aberrations are expected.

In configuration B, the Ritchey-Chretien telescope feeds a normal-incidence spectrometer with a VLS grating. A schematic layout of the optical configuration is shown in Fig. 1. The parameters of the telescope and consequently the resolution perpendicular to the slit are the same as in configuration A.

Grating	Spherical VLS
Central groove density	2400 lines/mm
Wavelength of operation	1160-1260 Å (first order) 580-630 Å (second order)
Entrance arm	1226 mm
Exit arm	1205 mm
Incidence angle	11.89°
Radius	1200 mm
Size	40 mm (⊥ to the grooves) × 105 mm
Coating	SiC
Detector	
Pixel size	10 μm
Format	2900 pixel × 3600 pixel
Area	29 mm (⊥ to the slit) × 36 mm
Spectral resolving element	35 mÅ (I order)
Spatial resolving element	0.55 arcsec

Tab. 2. Characteristics of the spectrometer in configuration B

The characteristics of the VLS grating are presented in Tab. 2. The grating has a groove density of 2400 lines/mm and entrance and exit arm of about 1200 mm. The parameters for groove space variation and the incidence angle have been optimized for having the lowest aberrations in the region 1160-1260 Å (580-630 Å) in the first (second) order. The incidence angle is 11.9°, making a subtended angle of 7° at the central wavelength. With respect to the configuration A, the subtended angle has been reduced by a factor of about two, so lower off-axis aberrations are expected. The spectral dispersion is 3.47 (1.74) Å/mm in the first (second) order.

The extension of the spectrum is 29 mm (in the plane of spectral dispersion) × 36 mm (in the direction parallel to the slit). This requires a detector array of 2900 × 3600 10 μm pixel. The spectral resolving element is 34.7 (17.4) mÅ in the first (second) order, which corresponds to a velocity resolution of 8.6 km/s. The spatial resolving element is 0.55 arcsec.

The spectral and spatial aberrations on the focal plane of the spectrometer are shown in Fig. 4, as calculated by a simulation of the whole optical system (telescope + spectrometer). The spectrum is almost stigmatic: the on-axis aberrations are lower than 10 μm within the spectral region to be acquired. Both spectral and spatial resolution are not preserved for off-axis points, but the degradation of the performance is much lower than the configuration A. The spectral and spatial resolutions are respectively degraded to 140 mÅ and 2.3 arcsec at ±17 arcmin.

A substantial improvement in the performance has been obtained with respect to the toroidal grating, due to the lower subtended angle. In any case, the high resolution given by the telescope in the direction parallel to the slit is not preserved for off-axis points.

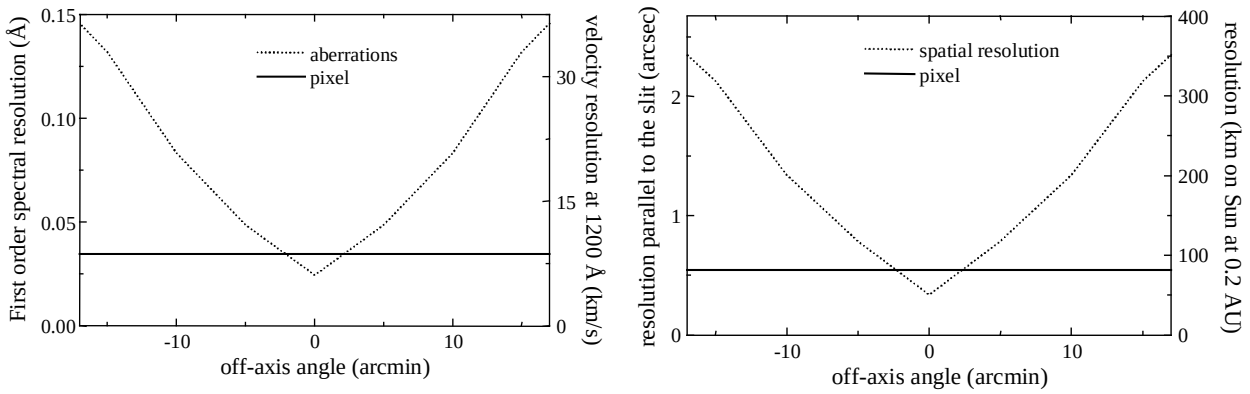

Fig. 4. Configuration B: spectral resolution and spatial resolution parallel to the slit. The pixel size is 10 μm.

3. Configuration C: grazing-incidence telescope and normal-incidence VLS-grating spectrometer

The configuration C consists on a grazing-incidence telescope with a field-of-view of 34 arcmin feeding a normal-incidence VLS-grating spectrometer. The advantages of using grazing-incidence optics are mainly the reduction of the thermal load and the increase in reflectivity, at the expense of an additional reflecting surface: in fact, a plane mirror for the rastering must be inserted between the telescope and the entrance slit. With respect to the normal-incidence telescope, the spatial resolution on the entrance slit is lower, due to the shorter focal length, but the optical performances on the focal plane are similar to those of the configuration B.

In the grazing-incidence domain, at least two reflecting surfaces are necessary to give an useful field-of-view obeying to the Abbe condition. Perfect on-axis images and a usable field are given by systems with two confocal conical mirrors, the so-called Wolter configurations. Among the three different designs of Wolter telescopes, type II is the more suitable for EUV observations with grazing angles of the order of 7-15°. It adopts a paraboloid and a hyperboloid arranged coaxially with a coincident common focus which makes the system focus; the two reflections occur in the internal surface of the paraboloid and on the external surface of the hyperboloid. The main advantage of Wolter II configuration is that the equivalent focal length can exceed the system length substantially. Note that the Wolter II is the grazing-incidence analogue of the Cassegrain normal-incidence telescope.

The optical layout is shown in Fig. 1. The primary and the secondary of the Wolter II telescope are separated by 200 mm, with the focal plane 1550 mm beyond the primary. The effective focal length is about 2.3 m. Giving a slit width of 10 μm, the region of the Sun imaged on the detector is a rectangular portion with angular size 0.9 arcsec (perpendicular to the slit) × 34 arcmin (parallel to the slit). The slit width has been fixed to a minimum width according to the optical aberrations and to the diffraction at 1200 Å.

An additional plane mirror for the rastering is inserted between the telescope and the slit. In this case, the spatial resolution on the slit is not fully preserved by the rastering. The resolution perpendicular to the slit for a rastering on 20 arcmin is shown in Fig. 6. In order to maintain a good spatial resolution, the field-of-view in the direction perpendicular to the slit has been reduced to 20 arcmin. The resolution is almost limited by the slit width to 0.9 arcsec (135 km on the Sun at 0.2 AU) within 10 arcmin. For a wider rastering, the resolution decreases at the extremes of the field-of-view in the direction parallel to the slit. Note that the spectrometer could share the same pointing mechanism as the high-resolution imagers, then it could have also the same field-of-view in the direction perpendicular to the slit, that is 8 arcmin. In this case, the resolution is fully limited by the slit width within the whole field-of-view.

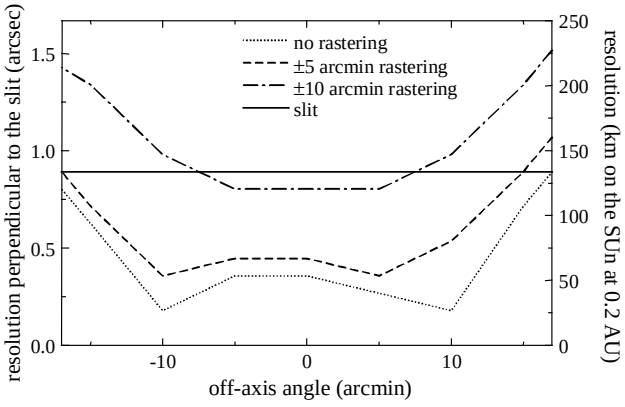

Fig. 6. Configuration C: spatial resolution perpendicular to the slit (9 μm wide).

Telescope	Wolter II
Field of view	34 arcmin (parallel to the slit, simultaneous) × 20 arcmin (⊥ to the slit, to be acquired by rastering)
Entrance aperture	
Size	55 mm × 55 mm
Primary mirror	Paraboloid
Size	200 mm × 55 mm
Incidence angle	74°
Secondary mirror	Hyperboloid
Distance from the primary	200 mm
Distance from the slit	1550 mm
Size	190 mm × 40 mm
Incidence angle	78°
Focal length	2310 mm
Mirror for the rastering	Plane
Distance from the slit	100 mm
Size	110 mm × 24 mm
Incidence angle	82°
Slit	
Size	10 μm × 23 mm
Spatial resolution ⊥ to the slit	0.9 arcsec
Grating	Spherical VLS
Central groove density	2400 lines/mm
Wavelength of operation	1160-1260 Å (first order) 580-630 Å (second order)
Entrance arm	600 mm
Exit arm	1200 mm
Incidence angle	10°
Radius	790 mm
Size	15 mm (⊥ to the grooves) × 45 mm
Coating	SiC
Detector	
Pixel size	18 μm
Format	1600 pixel × 2600 pixel
Area	29 mm (⊥ to the slit) × 47 mm
Spectral resolving element	62 mÅ (I order)
Spatial resolving element	0.8 arcsec

Tab. 3. Characteristics of the telescope-spectrometer in configuration C

The spectrometer has a spherical VLS grating with 2400 lines/mm optimized in the region 1160-1260 Å (580-630 Å) in the first (second) order. The exit arm is 1200 mm, corresponding to a spectral dispersion of 3.47 (1.74) Å/mm in the first (second) order. In order to reduce the size of the instrument, the entrance arm is fixed to 600 mm, giving a magnification of 2. The extension of the spectrum is 29 mm (in the direction of spectral dispersion) × 46 mm (in the direction parallel to the slit). This requires a detector array of 1600 × 2600 5 μm pixel. The spectral resolving element is 62 (31) mÅ in the first (second) order, which corresponds to a velocity resolution of about 16 km/s. The spatial resolving element is 0.8 arcsec.
The parameters of the telescope-spectrometer are summarized in Tab. 3.
The spectral and spatial aberrations on the focal plane of the spectrometer are shown in Fig. 6. The spectral aberrations are constant within the spectral region to be acquired. The on-axis aberrations (at 80% of the encircled energy) with a 10 μm slit are about 18 μm, because of the combined effects of the grating magnification and the residual grating aberrations. Both spectral and spatial aberrations are not fully preserved within the field-of-view. In particular, the spectral and spatial resolutions are respectively degraded to 240 mÅ (first order) and 3 arcsec at ±17 arcmin. The performances are slightly worse than those of configuration B. The spectral resolving element is lower, but the resolution can be increased by the centroiding. It will be shown that the main advantages of the grazing-incidence configuration are the lower thermal load and the higher effective area.

4. Effective area

The solar atmosphere is a very dynamic environment, with changes on all time-scales. The current EUV spectroscopic capability for solar studies provides raster cadences of the order of 10 minutes. Obviously, this has to be improved. If we aim at exposure times of 1 s or even less in modest lines we can achieve rastered images of a few minutes for reasonable areas.
The minimum exposure time is limited by the effective area of the telescope and by the intensity of the lines to be acquired. Once the areas of the mirrors have been fixed by the requirements on the maximum optical aberrations, the effective area is maximized by the choice of the coating. Unfortunately, the thermal environment of SOLO is

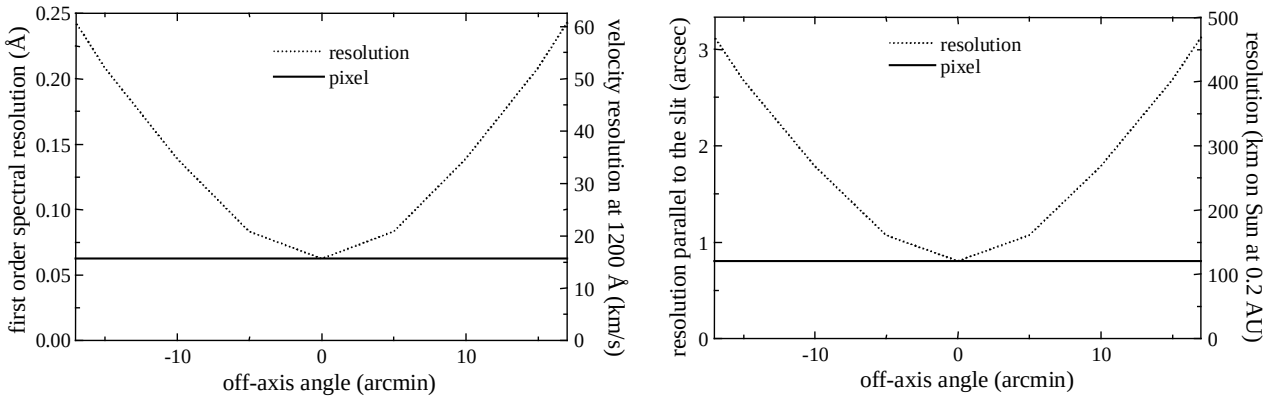

Fig. 6. Configuration C: spectral resolution and spatial resolution parallel to the slit. The pixel size is 18 μm.

particularly severe (the thermal load at 0.2 AU is 3.4 W/cm^2), so the coating must provide not only high reflectivity in the EUV, but also high reflectivity in the visible, in order to reduce the thermal absorption.

The EUV normal-incidence reflectivity, the corresponding effective areas of configurations A and B (calculated as the product of the illuminated section times the global efficiency) and the total power absorption are shown in Tab. 4 for some conventional EUV coatings. The solar irradiance curve has been taken equal to that of a blackbody at 5900 K. In the calculation of the effective area, the two reflections on the telescope, the grating efficiency and the detector efficiency have been taken into account. The grating and detector efficiencies have been supposed to be respectively 0.15 (in first and second orders) and 0.40.

The best performance in terms of reflectivity are given by SiC, at the expense of a very high absorption in the visible and IR (up to 80%). This makes very difficult to use SiC in optics looking at the Sun with very high thermal load. Reflectivity and also absorption are lower for metallic coatings, so in this case the power can be dissipated via a relatively small radiator.

It is worth to estimate the acquisition time of a single spectrum in order to evaluate the capability of the instrument to follow the evolution of fast dynamic processes on the solar surface. Let us suppose that the whole line is spectrally sampled by a single pixel, i.e. its spectral bandwidth is lower than the spectral resolving element. The fluxes collected by a pixel looking at a region on the Sun of 0.5 arcsec (in the direction perpendicular to the slit) × 0.55 arcsec (in the direction parallel to the slit) at 0.2 AU, with the effective areas as calculated in Tab. 4, are reported in Tab. 5. They are of the order of 10-15 counts/pixel/s in case of an emission intensity of 10^{13} photons/cm^2/sr/s, and 100-150 counts/pixel/s in case of an emission intensity of 10^{14} photons/cm^2/sr/s. It is clear that a good signal-to-noise ratio can be obtained in exposure times of few seconds only for very bright lines.

Obviously, the flux can be increased at the expense of a lower spatial resolution. Giving the limited budget in size and mass on SOLO, a trade-off between collected flux and spatial resolution has to be reached.

Coating	**Reflectivity at 600 Å**	**Reflectivity at 1200 Å**	**Effective area of configurations A and B at 600 Å** (cm^2)	**Effective area of configurations A and B at 1200 Å** (cm^2)	**Total absorption** (%)
Au	0.13	0.16	0.10	0.15	21
Ir	0.20	0.18	0.23	0.19	28
Pt	0.21	0.21	0.26	0.26	34
SiC	0.33	0.48	0.63	1.34	80

Tab. 4. EUV normal-incidence reflectivity, effective area of configurations A and B and total absorption of different coatings. The grating and detector efficiency have been supposed to be respectively 0.15 and 0.4.

Coating	**Flux at 600 Å with 10^{13} photons/cm^2/sr/s** (counts/pixel/s)	**Flux at 1200 Å with 10^{13} photons/cm^2/sr/s** (counts/pixel/s)	**Flux at 600 Å with 10^{14} photons/cm^2/sr/s** (counts/pixel/s)	**Flux at 1200 Å with 10^{14} photons/cm^2/sr/s** (counts/pixel/s)
Au	7	10	70	100
Ir	15	12	150	120
Pt	14	17	140	170

Tab. 5. Fluxes collected by a pixel (0.5 arcsec × 0.55 arcsec) in configurations A and B with metallic coatings. The whole spectral line is supposed to be sampled by a single pixel.

The EUV grazing-incidence reflectivity, the corresponding effective areas of configuration C and the total power absorption are shown in Tab. 6. The grating and detector efficiencies have been supposed respectively 0.15 and 0.4. With respect to the normal-incidence case, the reflectivity is higher and the power absorption is reduced. Very high EUV reflectivity and then high effective area are obtained by using Si or SiC at grazing incidence. Unfortunately, both the materials are partially transparent in the visible and IR, resulting in a very high absorption (of the order of 0.6 at 74°). In order to increase the reflectivity in the visible, the Si or SiC layer is deposited on a gold coating. The EUV reflectivity is unchanged, while the absorption is reduced down to 0.2. In this case, the effective area is a factor 5-10 higher than in the normal incidence case with metallic coatings. We plan to do some tests on such high reflective coatings.

In order to estimate the acquisition time of a single spectrum, let us suppose that the whole line is spectrally sampled by a single pixel. The fluxes collected by a pixel looking at a region on the Sun of 0.9 arcsec (in the direction perpendicular to the slit) × 0.8 arcsec (in the direction parallel to the slit) at 0.2 AU are reported in Tab. 7. When using Si coating, the flux is of the order of 200 counts/pixel/s in case of an emission intensity of 10^{13} photons/cm^2/sr/s. For such lines, the minimum exposure time can be even shorter than 1 s.

Coating	**Reflectivity At 600 Å (74°-78°-82°)**	**Reflectivity at 1200 Å (74°-78°-82°)**	**Effective area of configuration C at 600 Å** (cm^2)	**Effective area of configuration C at 1200 Å** (cm^2)	**Total absorption (74°-78°-82°)** (%)
Au	0.40-0.50-0.62	0.40-0.50-0.62	0.23	0.23	19-17-14
Ir	0.48-0.55-0.67	0.40-0.48-0.60	0.32	0.21	33-32-31
Pt	0.52-0.61-0.72	0.45-0.52-0.63	0.41	0.27	38-37-35
SiC (200 Å) + Au	0.78-0.83-0.88	0.59-0.64-0.72	1.03	0.49	26-22-17
Si (200 Å) + Au	0.80-0.85-0.90	0.80-0.84-0.89	1.11	1.09	22-21-19

Tab. 6. EUV grazing-incidence reflectivity, effective area of configuration C and total absorption of different coatings. The grating and detector efficiency have been supposed to be respectively 0.15 and 0.4.

Coating	**Flux at 600 Å with 10^{13} photons/cm^2/sr/s** (counts/pixel/s)	**Flux at 1200 Å with 10^{13} photons/cm^2/sr/s** (counts/pixel/s)	**Flux at 600 Å with 10^{14} photons/cm^2/sr/s** (counts/pixel/s)	**Flux at 1200 Å with 10^{14} photons/cm^2/sr/s** (counts/pixel/s)
Au	40	40	400	400
Ir	54	35	540	350
Pt	70	45	700	450
SiC (200 Å) + Au	174	83	1740	830
Si (200 Å) + Au	190	185	1900	1850

Tab. 7. Fluxes collected by a pixel (0.9 arcsec × 0.8 arcsec) in configuration C. The whole spectral line is supposed to be sampled by a single pixel.

5. Thermal load

The thermal environment of SOLO is particularly severe: at 0.2 AU the average solar intensity is 25 times the solar constant, i.e. ≈34 kW/m^2. The constraints due to the extreme and variable irradiation and thermal budget that the payload has to do with are very serious.

The thermal loads at 0.2 AU on the optics are reported in Tab. 8. The thermal loads are particularly severe for the normal-incidence telescope: the primary mirror absorbs 0.7-1.0 W/cm^2 and the secondary 2.2-3.0 W/cm^2. The power density is particularly high on the secondary because of the focusing from the primary. The power absorption is about 16 solar constants for gold and even more for other coatings. This gives some serious drawbacks:

1. the stability of the coating and the deformation of the optical surface have to be carefully analyzed;
2. the dissipation of such an high thermal flux is very problematic.

The extreme solar flux on the mirrors have another even more serious effect. It is well known that under high irradiation, particularly in the ultraviolet, any contaminant deposited on an optical surface, even in very minute amounts, polymerizes, so the reflectivity of the surface drastically decreases. The amount of the effect depends on the irradiation exposure and on the partial pressure of the contaminant. Even with the tightest procedures in handling and

assembling the optics, under the extreme irradiation conditions of the 0.2 AU orbit, there is a risk of a serious rapid degradation of the reflectivity.
Note that the extreme irradiation and thermal load makes the use of multilayer coatings, that allow high reflectivity for low wavelengths in normal incidence, very problematic. Therefore the mirrors and the grating must have metallic layers and this limits the spectral range of normal-incidence configurations to > 40 nm, eliminating any diagnostic capabilities for high temperature plasmas.
On the contrary, the thermal loads are relaxed for the grazing-incidence telescope: the power densities absorbed by the concave mirrors are 0.2-0.3 W/cm^2, considerably lower than the normal-incidence case. In this case, the stability of the coating and the deformation of the optical surfaces are less critical. Even lower is the power density absorbed by the plane mirror, about 0.04 W/cm^2.
Furthermore, the degradation of the reflectivity due to the residual contaminants is much less severe when the optics are operated in grazing incidence. Firstly, the portion of the optics illuminated at grazing incidence is much larger than in

	NORMAL-INCIDENCE TELESCOPE	**GRAZING-INCIDENCE TELESCOPE**
Primary mirror		
Percentage of the flux stopped by the tube	8 %	0%
Entrance aperture	133 cm^2	30 cm^2
Illuminated area	97 cm^2	110 cm^2
Thermal load at 0.2 AU	303 W (3.1 W/cm^2)	102 W (0.9 W/cm^2)
Absorption at 0.2 AU	Au: 64 W (0.7 W/cm^2) Ir: 85 W (0.9 W/cm^2) Pt: 103 W (1.1 W/cm^2)	Au: 19 W (0.2 W/cm^2) Ir: 34 W (0.3 W/cm^2) Pt: 39 W (0.4 W/cm^2) SiC: 27 W (0.3 W/cm^2) Si: 22 W (0.2 W/cm^2)
Secondary mirror		
Percentage of the flux arriving on the mirror	70 %	95 %
Illuminated area	16 cm^2	76 cm^2
Thermal load at 0.2 AU	Au: 167 W (10.4 W/cm^2) Ir: 153 W (9.6 W/cm^2) Pt: 140 W (8.8 W/cm^2)	Au: 79 W (1.0 W/cm^2) Ir: 65 W (0.9 W/cm^2) Pt: 60 W (0.8 W/cm^2) SiC: 75 W (1.0 W/cm^2) Si: 80 W (1.1 W/cm^2)
Absorption at 0.2 AU	Au: 35 W (2.2 W/cm^2) Ir: 43 W (2.7 W/cm^2) Pt: 48 W (3.0 W/cm^2)	Au: 13 W (0.2 W/cm^2) Ir: 21 W (0.3 W/cm^2) Pt: 22 W (0.3 W/cm^2) SiC: 17 W (0.2 W/cm^2) Si: 17 W (0.2 W/cm^2)
Plane mirror for rastering		
Percentage of the flux arriving on the mirror		10 %
Illuminated area		26 cm^2
Thermal load at 0.2 AU		Au: 6.6 W (0.3 W/cm^2) Ir: 4.4 W (0.2 W/cm^2) Pt: 3.8 W (0.1 W/cm^2) SiC: 5.8 W (0.2 W/cm^2) Si: 6.3 W (0.2 W/cm^2)
Absorption at 0.2 AU		Au: 0.9 W (0.04 W/cm^2) Ir: 1.4 W (0.05 W/cm^2) Pt: 1.3 W (0.05 W/cm^2) SiC: 1.0 W (0.04 W/cm^2) Si: 1.2 W (0.05 W/cm^2)

Tab. 8. Thermal load on the optics for the normal-incidence (A and B) and grazing-incidence (C) configurations.

normal incidence (for the same aperture) and correspondingly the flux decreases (this is beneficial also for cooling the optics); secondly, the effect of polymerization results in a much less decrease of the reflectivity than in normal incidence.

6. Conclusions

The optical design and performance of three different telescope-spectrometers for high-resolution solar imaging spectroscopy in the spectral region 1160-1260 Å (580-630 Å) have been presented. The layout consists essentially of a telescope and a normal-incidence stigmatic spectrometer.

It has been shown that the high resolution of a double-element telescope is degraded by the single-element spectrometer. The lower the subtended angle on the spectrometer, the better the off-axis performance. With regard to that, VLS-grating spectrometers can operate at lower incidence angle than toroidal-grating spectrometers, then they give definitely better off-axis performances.

From the optical point of view, the configuration B (normal-incidence telescope with VLS grating) is preferable with respect to the configuration C (grazing-incidence telescope with VLS grating). The spatial and spectral resolutions are higher, the field-of-view in the direction perpendicular to the slit is larger, and the off-axis performances are better.

The grazing-incidence configuration has higher effective area even with conventional metallic coatings. The area can be maximized with a different coating (silicon on gold), that we are going to test in the near future.

The grazing-incidence configuration is definitely preferable when analyzing the thermal load on the optics. In particular, the flux on the secondary mirror of a normal-incidence telescope is particularly high (about 70 solar constants), and this makes very difficult to operate the Ritchey-Chretien telescope without degradation in time due both to coating degradation and surface contamination.

Considering the severe environment of SOLO, we retain that grazing-incidence optics could satisfy the scientific requirements in a more robust and effective instrument.